In: Optimization in Polymer Processing ISBN # 978-1-61122-818-2
Editor: A.Gaspar-Cunha, J. A.Covas, pp.1-35

Chapter 6

REACTIVE EXTRUSION - OPTIMIZATION OF REPRESENTATIVE PROCESSES

***António Gaspar-Cunha*[*], *José Antonio Covas*[*],**
***Bruno Vergnes*[**], *Françoise Berzin*[***]**

[*] Institute for Polymers and Composites/I3N, University of Minho, Campus de Azurém, 4800-058 Guimarães, Portugal
[**]MINES ParisTech, Centre de Mise en Forme des Matériaux (CEMEF), UMR CNRS 7635, BP 207, 06904 Sophia Antipolis Cedex, France
[***] GRESPI, Université de Reims Champagne-Ardenne, Esplanade Roland Garros, BP 1029, 51586 Reims Cedex 2, France

Key words: Multi-Objective Optimization, Evolutionary Algorithms, Reactive extrusion optimization, Starch cationization, ε-caprolactone polymerization.

1 Introduction

Reactive extrusion consists in using an extruder as a continuous chemical reactor [1-3]. In parallel with the conventional functions of a screw extruder (solids conveying, melting, mixing, melt pumping), a chemical reaction

develops and must be controlled. In comparison with a classical chemical process in solution, reactive extrusion exhibits interesting advantages [3-4]:

- as the reaction is conducted in the melt, no solvent is required;
- contrarily to batch reactors, an extruder can work with very viscous products;
- extruders (namely twin screw extruders) can be very flexible (for example, allowing the sequential addition of the reaction ingredients, such as monomer, polymer, water, solvent, reactant, etc.) and simple to use due to the independency between feed rate and screw speed;
- can be easily attached to downstream equipment, for shaping or pelletization purposes.

Naturally, reactive extrusion has also some limitations:

- the residence time in an extruder is usually short (typically, of the order of a few minutes). Thus, even if the values of temperature and reagents concentration are higher in the melt than in solution, reactions have to be fast enough;
- highly exothermic reactions are difficult to control, due to the low cooling capacity of extruders (furthermore, this capacity decreases with increasing machine sizes).

Co-rotating intermeshing twin screw extruders are the most widely used in reactive extrusion, because they present a lot of advantages compared with single screw extruders:

- they have modular geometry, that is, it is possible to build the screw profile and the barrel configuration that are more adequate to the reaction to develop;
- they are starve fed, i.e., the feed rate is controlled by volumetric or gravimetric feeder(s). Consequently, the screws work mostly partially filled, which entails some additional benefits: i) it is possible to insert along the barrel different feeding ports, either for liquids or for solids, ii) devolatilization is easy in zones with a low filling ratio, iii) the screw profile can be divided into successive independent sections, with specialized functions (polymer feeding and melting, injection of reagents, mixing, reaction development, devolatilization, pumping and

shaping…) and iv) the residence time and the level of thermomechanical stresses are relatively easy to control;

- they have superior mixing capacities, both in distributive and dispersive terms. Mixing can be controlled by the geometry of certain screw sections (in general, blocks of staggered kneading discs) and by the operating conditions [5];
- the screws can rotate at high screw speeds (up to more than 1500 rpm), thus promoting high dispersion levels whilst guaranteeing high production rates;

Nowadays, many polymer systems are industrially manufactured using a reactive extrusion process [3, 6]:

- after initiation in a pre-polymerizer (batch reactor), styrene is usually polymerized in an extruder. Polyesters, polyamides, or polyacrylates, can also been produced by reactive extrusion;
- existing polymers can be chemically modified to offer new properties. For example, maleic anhydride can be grafted onto polypropylene. Other modifications, such as exchange reactions or modification of functional groups, can also be conducted via reactive extrusion;
- the degradation of polypropylene by peroxides is commonly used to control the molecular weight distribution and, therefore, the rheological properties;
- immiscible polymer blends can be efficiently compatibilized in-situ during compounding, by an interfacial reaction [1-3];
- thermoplastic elastomers are obtained by dynamic vulcanization, where the elastomer is dispersed and vulcanized in a thermoplastic matrix. The key point here is the phase inversion taking place during the vulcanization process.

This chapter is organized as follows. In section 2, the methodology used to model reactive extrusion is presented and the two chemical reactions selected (ε-caprolactone polymerization and starch cationization) are described in relative detail. Then, in section 3, the multi-objective optimization algorithm described in chapter 4 is applied to a few examples involving those chemical reactions and the results are presented and discussed. The chapter finishes with some conclusions.

2 Reactive Extrusion Modeling

2.1 Concepts

Reactive extrusion is at present an important method to modify and develop new polymeric materials. However, it is also a complex process, due to the high number of processing parameters and their possible interactions [7]. For example, increasing the screw speed will decrease the residence time and increase the melt temperature due to viscous dissipation, generating opposing effects on the reaction kinetics. Moreover, if the viscosity is affected by the reaction rate, in turn it will influence the flow conditions and, consequently, the reaction. In other words, since the understanding and the control of a reactive extrusion process addresses several difficult questions, it is important to develop theoretical approaches that may induce the development of computational tools with good predictive ability.

To model reactive extrusion, it is necessary to build various modules, to be subsequently coupled into an algorithm:

a) calculation of the flow in the extruder (this chapter deals exclusively with co-rotating twin screw extruders, the most common for reactive extrusion; Chapter 5 contains an introduction to the geometry, working characteristics and flow modeling of this type of machines);
b) calculation of the chemical reaction;
c) eventual physical and rheological changes induced in the material by the chemical reaction.

Flow in the Twin screw extruder

Obviously, it is necessary to predict, as accurately as possible, the flow conditions along the twin screw extruder. Both the geometry and the kinematics in this machine are complex and the flow is strongly unsteady, non-isothermal and three-dimensional. Thus, in order to derive a global model taking into account the whole process from hopper to die exit with reasonable computational costs, simplifications are necessary.

More than ten years ago, the Ludovic© program was developed at CEMEF [8]. It is based on a local 1D approach and calculates the main flow parameters (temperature, pressure, shear rate, viscosity, residence time, etc) along the extruder. The computations are performed separately for each type of element (partially or totally filled right-handed screw elements, left-handed screw elements, blocks of kneading disks). For screw elements, pressure/flow rate

relationships are determined assuming a rectangular channel cross-section with constant width and taking into account the wall effects by means of correcting factors. For kneading blocks, the peripheral flow around each individual disk is taken into consideration; this is characterized by a pressure peak located ahead of the disk tip. The staggering of the tips of adjacent disks induces a staggering of the pressure profiles, thus creating an axial pressure gradient that pushes the material into the axial direction. The preceding elementary models are linked together to obtain a global description of the flow field along the extruder. A melting model has also been developed [9], but one can simply assume that instantaneous melting takes place in the first restrictive element of the screw. After melting, the polymer fills totally or partially the screw channel, depending on the local geometry and flow conditions. Experimental validations and intensive use of the Ludovic© software in many applications have shown its ability to depict adequately the flow conditions inside a twin screw extruder [10-13].

Recently, the Twixtrud program has been put together at University of Minho [14]. It takes into account the different physical steps occurring along the extruder, that is, solids conveying (devoid of or under pressure), delay in melting, melting (initially with high solids content, then under low solids content) and melt conveying (also without or under pressure). As the solid polymer is supplied at a constant rate by a feeder, it progresses axially along the partially filled screw channels, following the well-known figure-of-8 flow pattern. When a restrictive element is reached, the polymer fills up the channel and pressure is generated to overcome the restriction imposed. This pressure, together with the rising local temperatures, brings about the formation of a solid plug exposed to heat conduction from all surrounding surfaces (screw and barrel). A melt film is created when the temperature of the polymer close to the barrel reaches its melting point; the thickness of this melt increases until a melt pool forms near to the active screw flight a few centimeters downstream. Then, melting develops in two stages: initially, the solid plug is surrounded by the melt films and the melt pool, which grows in size. When the solid content is low enough, the solid plug rips open, so that it transforms into a number of solid particles suspended in the melt, their size decreasing progressively along the screw due to heat conduction from the melt. When melting is completed, the flow progresses in filled or partially filled channels, depending on the local geometry and on the operating conditions, until it exits the die.

The main differences between Ludovic© and TwiXtrud are related to the different handling of melting and to the inclusion (by the latter) of solids

conveying. Furthermore, TwiXtrud calculates a temperature profile across the channel, while Ludovic© computes a mean temperature. The two programs will be used in the optimization examples below.

*Chemical r*eaction

The development of a chemical reaction is described by kinetic equations, involving kinetic constants. Once the reaction scheme is known, balance equations can be written for the various existing chemical species, in order to define a degree of conversion as a function of time and temperature. Depending on the reaction complexity, the kinetics can be described by either a simple analytical function or by a set of partial differential equations. Two examples will be presented in sections 2.2 and 2.3.

The difficulty in implementing this computational module is to derive the correct kinetic scheme and, accordingly, to obtain accurate values for the kinetic constants. In some cases, a small error in the characterization of the constants may induce large discrepancies in the simulation of the reactive extrusion process [15].

Rheokinetics

In the case of exchange reactions (for example, the starch cationization reaction that will be analyzed in section 2.3), the modifications on the polymer rheological behavior induced by the reaction can be neglected. In other words, the behavior of the initial polymer can be considered all along the extrusion process. However, when polymerization reactions occur (to be seen in section 2.2), the viscosity may increase along the extruder by six orders of magnitude (typically, from 10^{-3} to 10^{3} Pa.s). It is then necessary to take into account rheokinetic models, which describe the change in viscosity (and eventually in other material parameters) as a function of the conversion rate.

Coupling the various modules

When a rheokinetic module is taken in, the various calculation modules presented above have to be coupled: the reaction rate increases according to the local values of temperature and residence time, affecting the polymer viscosity which, in turn, modifies the local flow conditions (pressure, temperature…). The following procedure may be followed: a first calculation is carried out without coupling, in order to gather an estimation of residence times, temperatures and reaction extents. The local viscosity is then calculated

from these values. Then, a second calculation is performed, now coupling, at each location along the screws, the flow conditions, the reaction development and the corresponding viscosity. More detailed information can be consulted elsewhere [16].

Open challenges to model reactive extrusion

Since the modeling methodology of reactive extrusion proposed here is obviously based on a number of approximations, important questions remain open for discussion:

- the kinetic constants are generally measured under static and isothermal conditions. Are their values still valid for the conditions existing in the extruder?
- the reactive medium is assumed to be homogeneous and the reagents instantaneously perfectly mixed with the molten polymer. In practice, when dealing with products with very different viscosities, local mixing has probably to be taken into account;
- reagents degradation and side reactions induced by the high temperatures are difficult to be included in the model;
- the examples shown hereafter concern single phase materials. For example, in the case of reactive blends [2], the evolution of the morphology (dispersed or co-continuous phase, dimensions of droplets, or fibrils) has also to be accounted for. It would be necessary to develop an extra module for predicting the morphology [13] and to couple it with the existing ones.

Anyway, the modeling methodology proposed here was developed for over ten years and has been successfully applied to a large number of situations, including polymerization [15], controlled degradation [16, 17] and chemical modifications [18-21]. The next two sections will focus on two reactions that will be subsequently considered for optimization: i) the polymerization of ε-caprolactone, which requires a strong coupling between reaction development and viscosity changes, and ii) the cationization of starch, a chemical modification which has no influence on the rheological properties.

2.2 ε-caprolactone polymerization

Polymers and copolymers of ε-caprolactone are mainly used for medical applications, because they are biodegradable and generally biocompatible. They find application as biodegradable sutures, artificial skin, resorbable prostheses and sustained drug release systems. The bulk polymerization of ε-caprolactone can be initiated by different organometallic compounds, such as metal alkoxides, metal halides and carboxylates. A two step "coordination-insertion" process is generally assumed [22].

The bulk polymerization of ε-caprolactone during a twin screw extrusion reactive process is considered here. The initiator selected is a tetrapropoxy-titanium. The polymerization mechanism consists in monomer coordination onto the initiator, followed by monomer insertion into the titanium-alkoxy bond. A selective acyl-oxygen bond scission is observed during the ring opening (Fig. 1). Then, the polymer chain grows from the titanium atom by successive monomer insertion. This polymerization is living, as long as the reactive sites are not destroyed.

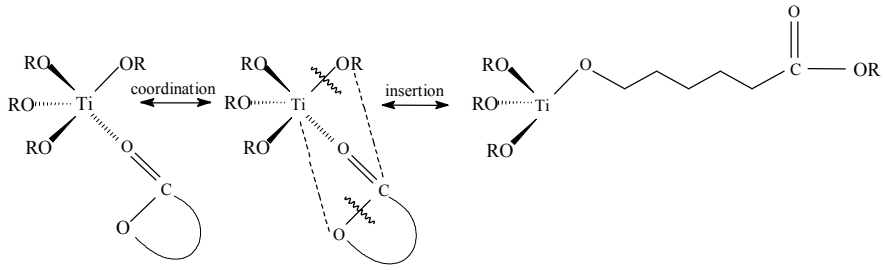

Figure 1. Reaction scheme of ε-caprolactone polymerization.

A global kinetic equation was proposed by Gimenez *et al.* [23-24]. The change in monomer concentration, [*M*], with time can be written as:

$$\frac{d[M]}{dt} = -K[M] \tag{1}$$

where the kinetic constant, *K,* is expressed as :

$$K = k\,[I_0]^{\alpha_c}\,\exp(-\frac{E_a}{RT}) \quad . \tag{2}$$

In this equation, k is a constant, $[I_0]$ the initial initiator concentration, α_c the partial order related to the initiator, E_a the activation energy, R the universal gas constant and T the absolute temperature. The monomer conversion, C, is defined as:

$$C = \frac{[M_0]-[M]}{[M_0]} \tag{3}$$

where $[M_0]$ is the initial monomer concentration.

By integrating equation (1), the variation of the monomer conversion with time is obtained:

$$C(t) = 1 - \exp(-K\,t). \tag{4}$$

From the conversion rate, the weight average molecular weight can be determined, using a linear relationship [24]:

$$\bar{M}_w = K^* C + \bar{M}_0 \tag{5}$$

where $\overline{M}_0$ is the molecular weight of the monomer and K^* is a constant depending on the initial $[M_0]/[I_0]$ ratio (monomer to initiator concentration ratio). Thus, the variation of the average molecular weight can be correlated to the conversion rate. Moreover, when $[M_0]/[I_0]$ increases, the kinetics is slower but the molecular weight increases.

Obviously, the polymerization reaction induces a huge increase in viscosity along the extruder, typically from 10^{-3} to 10^3 Pa.s. Detailed rheological studies were carried out by Gimenez *et al*. [25-26]. During polymerization, the viscoelastic parameters are strongly affected by the dilution effect due to the presence of monomers. Thus, the rheological behavior during polymerization is controlled by two regimes, the transition between them occurring at a critical molecular weight that is a function of polymer concentration:

$$M_c^* = M_c\, C^{-1.25} \tag{6}$$

where M_c is the critical polymer molecular weight. For $\overline{M}_w \le M_c^*$, a Rouse regime is assumed and the viscosity is Newtonian:

$$\eta = k_0\, a_T M_w^{1.2}\, a_c\, C \tag{7}$$

where a_T is the temperature shift factor, a_c is the free volume correction [26] and k_0 a constant.

For $\overline{M}_w > M_c^*$, an entangled regime is assumed. The viscosity is then defined by a Carreau-Yasuda equation:

$$\eta = \eta_0 \left[1 + (\lambda \dot{\gamma})^a\right]^{(n-1)/a} \tag{8}$$

where η_0 is the zero shear viscosity, λ a characteristic time, n the power law index and a the Yasuda parameter. The zero shear viscosity, η_0, and the characteristic time, λ, are a function of temperature, molecular weight and concentration of the polymer into its monomer, according to:

$$\eta_0 = A \exp\left[\frac{E_v}{R}\left(\frac{1}{T} - \frac{1}{T_0}\right)\right] M_w^{\alpha_v} C^4 a_c \tag{9}$$

$$\lambda = B \exp\left[\frac{E_v}{R}\left(\frac{1}{T} - \frac{1}{T_0}\right)\right] M_w^{\alpha_t} C^{1.75} a_c \tag{10}$$

where E_v is an activation energy and α_v and α_t two constants.

Coupled equations (1) to (10) characterize the kinetics and the evolutionary rheological behavior of polycaprolactone during polymerization. As explained before, for modeling purposes a two-step procedure is adopted:

- a first backwards calculation is performed from the die exit towards the hopper, using the rheological properties of the polymerized polycaprolactone, to provide a first estimation of the temperature profile and of the filled and partially filled sections of the extruder;
- then, a second forward calculation is carried out where, in each screw profile sub-element, the following coupling is performed:
  - from the local values of residence time and temperature, conversion along the sub-element is computed (Eq. 4);
  - this conversion defines a new molecular weight (Eq. 5) and then a new viscosity (Eq. 7 or 8);
  - from the new viscosity, the new pressure gradient (solving the flow equations) and the new temperature (solving the heat transfer equation) are calculated in the next sub-element. The thermal balance includes the reaction exothermicity, according to:

$$\Delta\overline{T} = \frac{1}{\rho C_p Q}\left[h_b S_b\left(T_b - \overline{T}\right) + h_s S_s\left(T_s - \overline{T}\right) + \dot{W} + \rho Q \Delta H \Delta C\right] \tag{11}$$

where $\Delta\overline{T}$ is the temperature change along a sub-element, ρ the density, C_p the heat capacity, Q the volumetric feed rate, h_b and h_s the heat transfer coefficients towards barrel and screw, S_b and S_s the corresponding exchange surfaces, T_b and T_s the barrel and screw temperatures, $\dot{W}$ the dissipated power, ΔH the reaction enthalpy and ΔC the change in conversion rate along the sub-element.

Figures 2 and 3 present an example of the results produced by the Ludovic© software, for polymerization under fixed processing conditions (screw speed N = 100 rpm, flow rate Q = 3 kg/h). Fig. 2 shows how temperature and cumulative residence time evolve axially. Temperature increases rapidly, essentially by heat transfer from the barrel, until reaching the barrel temperature. A further increase takes place at the die, where the viscosity attains its maximum (see Figure 3) due to viscous dissipation and reaction exothermicity. The residence time increases mainly in the kneading blocks and in the die, which has a large free volume.

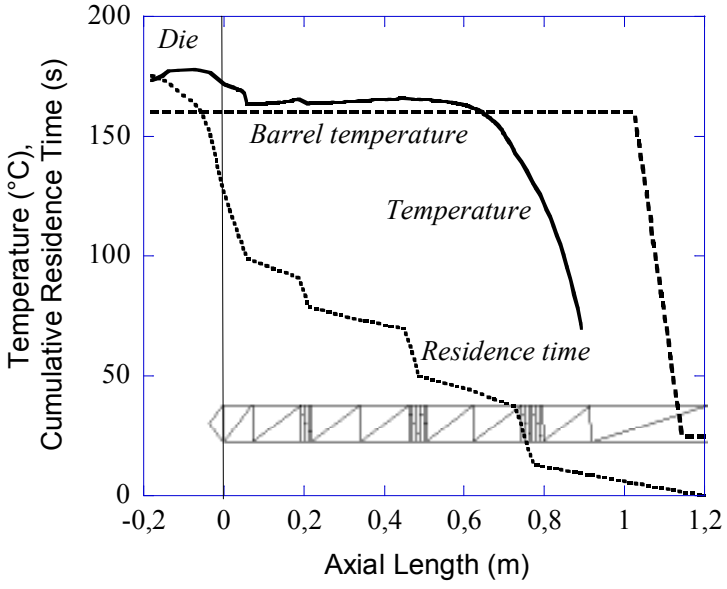

Figure 2. Changes in temperature and cumulative residence time along the screws. Reprinted from [15], with permission

Figure 3 depicts the corresponding changes in conversion rate and viscosity along the screw axis. The calculations begin just ahead of the first block of kneading discs, where the reagents are injected. As the temperature remains constant after the injection point, the conversion rate follows approximately the evolution of the residence time and is complete at the end of the screws. It is worth remarking the huge variation in viscosity along the extruder, from 10^{-4} to 10^{3} Pa.s.

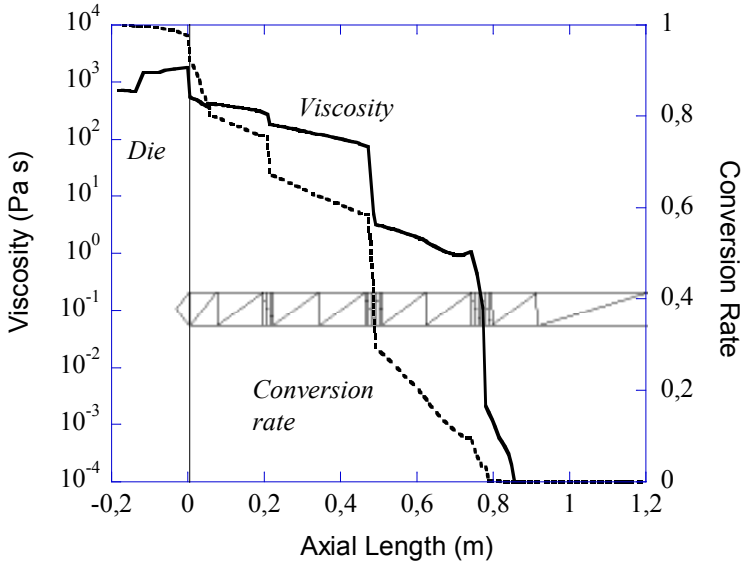

Figure 3. Changes in viscosity and conversion rate along the screws. Reprinted from [15], with permission

2.3 Starch Cationization

Starch is a polysaccharide largely applied in food and non-food packaging applications. Modified starches are widely used for paper, adhesives, textile, cosmetics and pharmaceutical products, among others [27]. Starch cationization is one of the most important starch modifications. In the paper-

making industry, cationic starches can increase the strength, filler and fines retention, as well as the pulp drainage rate. Sizing agents based on cationic starches present advantages due to their ionic attraction to cellulose fibers.

Starch cationization consists of the substitution of the hydroxyl groups of the glycosyl units by amino, ammonium, sulfonium, or phosphonium groups, able to carry a positive charge [28]. The degree of substitution, DS, indicates the average number of sites per anhydroglucose unit on which there are substituent groups. As there are three hydroxyl groups in each anhydroglucose unit, the maximum degree of substitution is 3. Usually, cationic starches used in the paper industry have DS between 0.02 and 0.05. In a previous experimental study [29], some of the authors used wheat starch plasticized with 40% water (on dry basis) and 2,3-epoxypropyltrimethylammonium chloride (commercialized as Quab© 151) as reagent. The reaction is shown in Figure 4.

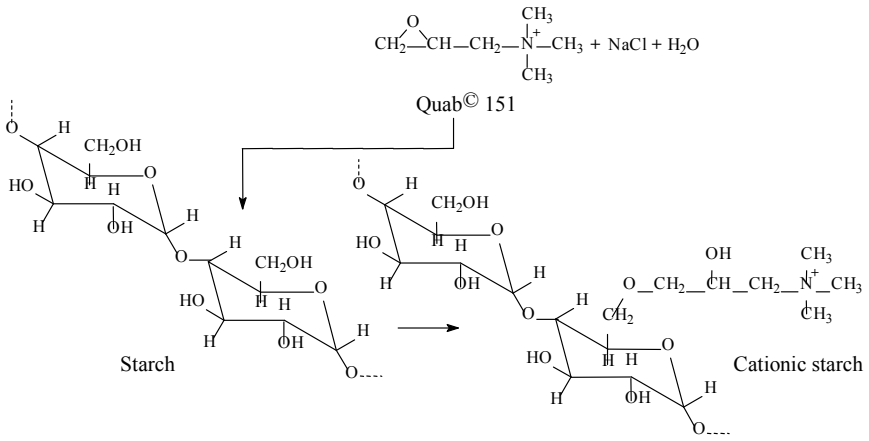

Figure 4. Reaction scheme of starch cationization.

The theoretical degree of substitution, DS_{th}, is the value corresponding to a reaction efficiency of 100%. DS_{th} is the molar ratio between reagent and anhydroglucose monomer and, in the experiments, it defines the target to reach; it also allows adjusting the values of the starch and reagent flow rates. The effective degree of substitution, DS, is estimated on extruded samples, by measuring the nitrogen content by a Kjeldahl method. The reaction efficiency, RE, is defined by DS/DS_{th}.

The kinetic scheme of starch cationization can be written as follows, considering a second order reaction [30]:

$$A + B \xrightarrow{k} C$$

Starch S-OH + Reagent (Quab©151) → Cationic starch S-O-R^+Cl^-

$$-\frac{d[A]_t}{dt} = -\frac{d[B]_t}{dt} = \frac{d[C]_t}{dt} = k[A]_t[B]_t \tag{12}$$

Expressing the reagent concentration $[B]_t$ as a function of that of the starch hydroxyl groups $[A]_t$, and of the initial concentrations, $[A]_0$ and $[B]_0$, and integrating, the following equation is obtained [30]:

$$[A]_t = \frac{\frac{[A]_0}{[B]_0}\left([A]_0 - [B]_0\right)\exp\left[k\left([A]_0 - [B]_0\right)t\right]}{\frac{[A]_0}{[B]_0}\exp\left[k\left([A]_0 - [B]_0\right)t\right] - 1} \tag{13}$$

The theoretical degree of substitution is:

$$DS_{th} = 3\frac{[B]_0}{[A]_0} \tag{14}$$

and the relationship between degree of substitution and starch concentration is:

$$DS = 3\frac{[C]_t}{[A]_0} = 3\frac{[A]_0 - [A]_t}{[A]_0} = \frac{DS_{th}}{[B]_0}\left([A]_0 - [A]_t\right) \tag{15}$$

As the reaction does not change significantly the native starch structure, one may assume that the cationization reaction does not modify the starch viscosity. In fact, this has been experimentally confirmed [31]. Consequently, in this case the viscous behavior can be simply described by a thermodependant power law.

In the experiments performed, it has been shown that DS or RE decrease with feed rate and increase with screw speed, barrel temperature and restrictive character of the screw profile (expressed in terms of the number of kneading blocks) [29]. All these experiments were simulated using the reactive version of Ludovic©, with the kinetic scheme presented above [19, 20]. Figure 5 summarizes the data: whatever the screw profile, the processing conditions and the reagent used (a second reagent, Quab© 188, was also tested), the

agreement between the calculated and measured reaction efficiencies is excellent.

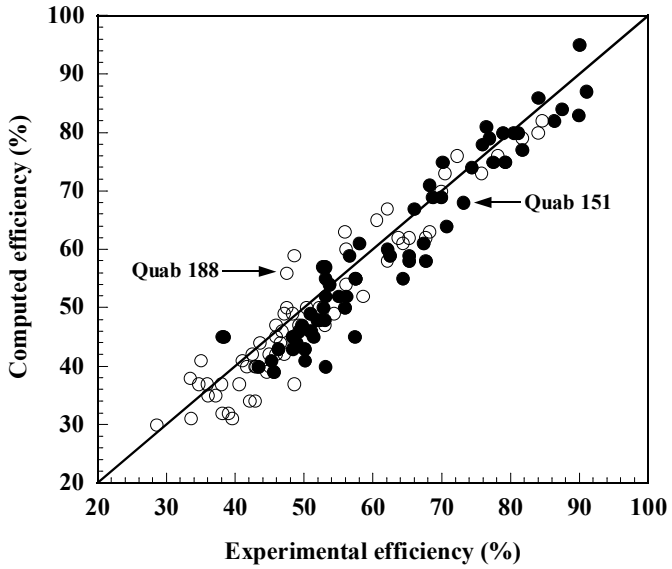

Figure 5. Comparison between calculated and measured reaction efficiency. Reprinted from [19], with permission.

3 EXAMPLES OF THE OPTIMIZATION OF REACTIVE EXTRUSION

3.1 Optimization Algorithm

The Multi-Objective Evolutionary Algorithm, MOEA, described in Chapter 4, can be applied to tackle the case studies discussed below. It is worth reminding that it consists of a modified version of the Reduced Pareto Set Genetic Algorithm, RPSGA, in order to be able to deal with the discrete characteristics of the twin-screw configuration problem (see explanation in Chapter 5).

The RPSGA parameters used are identical for the two chemical reactions, except for the number of generations studied (50 for ε-caprolactone polymerization, 30 for starch cationization). The main and elitist populations

had 100 and 200 individuals, respectively. A roulette wheel selection strategy, a crossover probability of 0.8, a mutation probability of 0.05, 30 ranks and limits of indifference of the clustering technique all equal to 0.01 were chosen (see Chapter 5 for more details).

The global aim of the optimization examples is to define the best operating conditions and/or screw configurations yielding the best process performance (quantified in terms of the minimization of the average melt temperature, specific mechanical energy and viscous dissipation and the maximization of output and average strain) and assuring the complete chemical conversion of the reactions involved. In the case of ε-caprolactone polymerization, process modeling was performed using the Ludovic software, while modeling of starch cationization was made with the TwinXtrud software.

3.2 ε-Caprolactone Polymerization

Table 1 summarizes the optimization runs performed for this reactive extrusion process. They can be classified in three groups. Group 1 (runs 1 to 4) concerns the optimization of the screw configuration. Group 2 (runs 5 to 8) aims at optimizing simultaneously the output and the screw configuration. Finally, in the third group (runs 9 to 12) the full set of operating conditions (i.e., output, screw speed and barrel temperature) and the screw configuration are optimized concurrently. Every run considers two objectives at once, the associated aim of the optimization and range of variation for each being defined in Table 2. The solutions for groups 2 and 3 (runs 5 to 12) are taken as valid only if the conversion rate (CR) is higher than 99.9%.

As for the screw configuration, the aim is to define the best axial location of the 10 screw elements identified in Table 3 with numbers 1 to 10. Four screw elements (two at the beginning and two at the end of the screw profile, respectively) are maintained at their original locations, due to the need to ensure enough conveying capacity in the initial process stages, as well as pressure generation upstream of the die. The diameter D, and the overall L/D are compatible with those of an existing Leitritz LSM 30-34 laboratory modular extruder.

Table 1. Optimization runs for ε-caprolactone polymerization.

Group	Run	Decision Variables				Objectives
		Q (kg/hr)	N (rpm)	T_b (ºC)	Screw Configuration	
1	1	10	100	190	10 elements	T_{exit}, *CR*
	2					*SME, CR*
	3					T_{max}/T_b, *CR*
	4					*AvgStrain, CR*
2	5	[3-30]	100	190	10 elements	Q, T_{exit}
	6					Q, *SME*
	7					Q, T_{max}/T_b
	8					Q, *AvgStrain*
3	9	[3-30]	[50-200]	[140-220]	10 elements	Q, T_{exit}
	10					Q, *SME*
	11					Q, T_{max}/T_b
	12					Q, *AvgStrain*

The initial monomer has a melt density of 1030 $kg.m^{-3}$, a melting point of 70ºC, a specific heat of 1700 $J.kg^{-1}.K^{-1}$, and a thermal conductivity of 0.2 $W.m^{-1}.K^{-1}$. Depending on the critical molecular weight, the viscosity is either defined by a Newtonian law (equation 7) or by a Carreau-Yasuda law (equation 8), in this case exhibiting a complex dependence on temperature, shear rate, molecular weight and concentration, as described in section 2.1 (equations 9 and 10). The values used for the constants in these equations are: $k_0 = 2.24\ 10^{-5}$, $a = 1.05$, $n = 0.52$, $A = 1.35\ 10^{-17}$, $B = 1.7\ 10^{-20}$, $E_v = 40$ $kJ.mol^{-1}$, $\alpha_v = 4.4$, $\alpha_t = 4.1$ and $T_0 = 413$ K.

Table 2. Optimization objectives, aim of optimization and range of variation.

Objective	Aim	Range of variation
Output (Q), kg/hr	Maximize	[3-30]
Temperature at die exit (T_{exit}), ºC	Minimize	[140-240]
Specific Mechanical Energy (*SME*), MJ/kg	Minimize	[0.1-2]
Viscous dissipation (T_{max}/T_b)	Minimize	[0.5-1.5]
Average strain (*AvgStrain*)	Maximize	[1000-15000]
Conversion rate (*CR*), %	Maximize	[0-100]

Figure 6 shows the initial and the final (50^{th} generation) non-dominated solutions for the optimization of the screw configuration - runs 1 to 4. It is clear that the initial solutions generated randomly evolve towards better solutions with higher performance, even if the operating conditions were maintained constant. The highest conversion rates are attained at the cost of deteriorating the remaining optimization objectives, i.e., of increasing T_{exit}, *SME* and viscous dissipation and of decreasing the average strain. This is not surprising, since the reaction is accelerated when the temperature is increased.

Table 3. Individual screw elements used in the optimization of ε-caprolactone polymerization (*L* is length, *P* is pitch, KB 30 indicates a block of kneading discs with a staggering angle of 30º; the thickness of the kneading disks is 7.5 mm)

Element	**Beginning of screw**		**1**	**2**	**3**	**4**	**5**	**6**	**7**	**8**	**9**	**10**	**End of screw**	
L (mm)	307	120	120	120	120	120	22.5	22.5	22.5	22.5	15	22.5	120	67.5
P (mm)	20	45	20	30	45	30	KB 30	KB 30	KB 30	KB 30	KB 30	KB 30	20	30

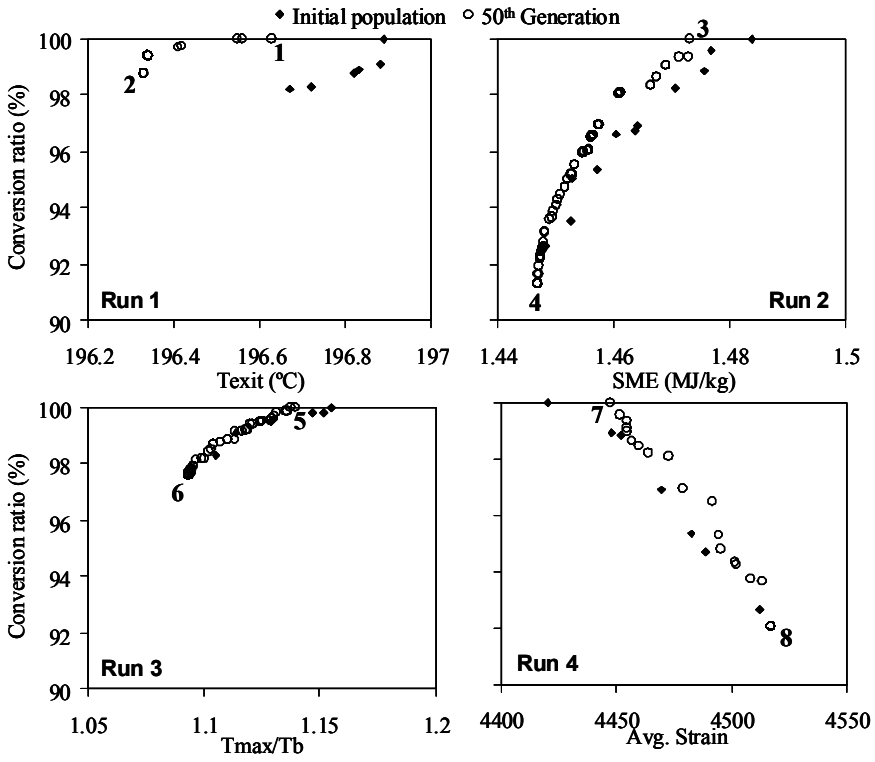

Figure 6. Pareto frontiers for group 1 (runs 1 to 4).

The points 1 to 8 in Figure 6 identify the solutions (that is, the screw configurations) that improve each of the objectives dealt with in each run. For example, point 1 indicates the solution that maximizes the conversion rate, *CR*, while point 2 shows the one that minimizes $T_{exit.}$. These screw configurations are detailed in Table 4. The optimization algorithm locates the first restrictive element as early as possible in the screw shaft (positions 1 or 2). Probably, since these types of elements increase the local residence times and temperature, the polymerization reaction will start as early as possible. However, the justification of the choices made by the algorithm to locate the remaining restrictive elements is not always evident. In fact, it would require an analysis of the changes of all the calculated data along the various screw profiles (pressure, temperature, residence time, conversion rate…), which obviously lies beyond the scope of the present text.

Table 4. Optimal screw configurations for the eight solutions identified in figure 6, runs 1 to 4.

Point		Beginning of screw		1	2	3	4	5	6	7	8	9	10	End of screw	
1	*L* (mm)	307	120	120	15	120	22.5	120	22.5	22.5	120	22.5	22.5	120	67.5
	P (mm)	20	45	30	KB 30	20	KB 30	30	KB 30	KB 30	45	KB 30	KB 30	20	30
2	*L* (mm)	307	120	22.5	120	120	120	22.5	22.5	22.5	120	22.5	15	120	67.5
	P (mm)	20	45	KB 30	30	20	45	KB 30	KB 30	KB 30	30	KB 30	KB 30	20	30
3	*L* (mm)	307	120	22.5	120	120	22.5	22.5	120	15	22.5	22.5	120	120	67.5
	P (mm)	20	45	KB 30	30	20	KB 30	KB 30	30	KB 30	KB 30	KB 30	45	20	30
4	*L* (mm)	307	120	120	22.5	120	22.5	22.5	22.5	120	22.5	15	120	120	67.5
	P (mm)	20	45	20	KB 30	45	KB 30	KB 30	KB 30	30	KB 30	KB 30	30	20	30
5	*L* (mm)	307	120	120	22.5	22.5	22.5	120	120	15	22.5	22.5	120	120	67.5
	P (mm)	20	45	30	KB 30	KB 30	KB 30	20	30	KB 30	KB 30	KB 30	45	20	30
6	*L* (mm)	307	120	120	22.5	120	22.5	120	120	22.5	22.5	22.5	15	120	67.5
	P (mm)	20	45	30	KB 30	30	KB 30	20	45	KB 30	KB 30	KB 30	KB 30	20	30
7	*L* (mm)	307	120	120	22.5	22.5	120	120	120	15	22.5	22.5	22.5	120	67.5
	P (mm)	20	45	20	KB 30	KB 30	30	45	30	KB 30	KB 30	KB 30	KB 30	20	30
8	*L* (mm)	307	120	120	22.5	120	120	22.5	22.5	22.5	22.5	120	15	120	67.5
	P (mm)	20	45	20	KB 30	45	30	KB 30	KB 30	KB 30	KB 30	30	KB 30	20	30

Following the same reasoning for the computational results of group 2, Figure 7 shows the non-dominated solutions of the initial and final populations for runs 5 to 8, i.e., when the output is optimized together with the screw configuration, whilst ensuring that all the solutions generated a conversion rate of at least 99.9%. Evidently, the Pareto frontiers of Figure 7 are different from those of Figure 6, because the output could now be varied. For example, in the case of run 5 lower temperatures could be attained, because lower outputs could be set. Exit and maximum temperatures increase with output, probably due to higher viscous dissipation, while the average strain decreases due to the shorter residence time. Run 6 aims at maximizing the output and minimizing SME. As the latter varies linearly with the ratio N/Q (screw speed/output) at fully filled zones (which are those that contribute more significantly to SME), these objectives are not conflicting and there is no further gain in varying the output. Consequently, the length of the Pareto frontier is reduced to only a few points.

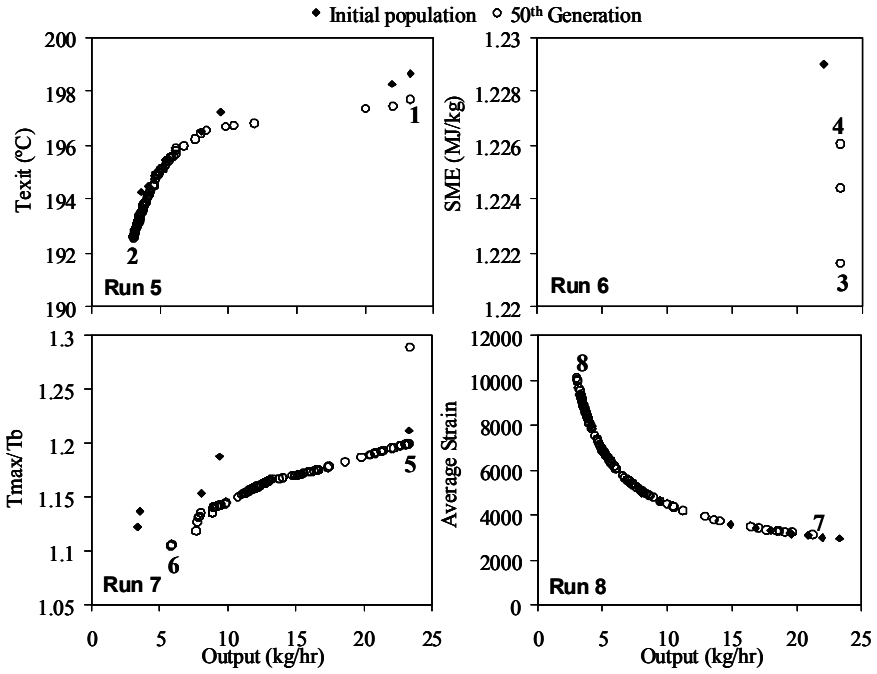

Figure 7. Pareto frontiers for group 2 (runs 5 to 8).

If the solutions that improve each of the objectives dealt with in each run are identified (points 1 to 8 in Figure 7), the corresponding screw configurations and output can be defined (see Table 5). Some solutions attain significant outputs, of up to more than 23 kg/hour. Experimental practice has demonstrated that this is indeed the practical limit of the Leistritz twin screw extruder, since under these conditions the screws work fully filled and/or the maximum motor Amperage is attained. Nevertheless, the explanation of the optimized profiles for the different runs is far from evident. This also means that an optimization design solely based on empirical knowledge, or on direct modeling, would have little probability of finding screw designs with this level of performance.

In group 3 (runs 9 to 12 in Table 1), the screw profile and the operating parameters (Q, N, T_b) are optimized at the same time. Table 6 shows the optimal solutions for this third group, where:

- for run 9, points 1 and 2 indicate the solutions that maximize output, Q and minimize $T_{exit.}$, respectively;
- for run 10, points 3 and 4 indicate the solutions that maximize Q and minimize SME, respectively;
- for run 11, points 5 and 6 indicate the solutions that maximize Q and minimize Tmax/Tb, respectively;
- for run 12, points 7 and 8 indicate the solutions that maximize output Q and average strain, *AvgStrain*, respectively.

The maximum screw speed is systematically chosen when the objective is to maximize output. When the exit temperature and SME are to be minimized, a low screw speed is chosen (57 and 59 rpm), which implies a very low output (to avoid the screws becoming fully filled). Barrel temperature is low when the exit temperature is to be minimized, but it is fixed at its maximum value to minimize SME, as the viscosity is at its lowest level under these conditions. To maximize strain, high screw speed and low output are imposed, which is perfectly reasonable, as the strain varies according to the N/Q ratio.

Table 5. Optimal screw configurations and output for the eight solutions identified in figure 7, runs 5 to 8.

Point		Beginning of screw		**1**	**2**	**3**	**4**	**5**	**6**	**7**	**8**	**9**	**10**	End of screw		***Q*** (kg/hr)
1	*L* (mm)	307	120	120	15	22.5	22.5	22.5	120	120	120	22.5	22.5	120	67.5	23.3
	P (mm)	20	45	30	KB 30	KB 30	KB 30	KB 30	30	20	45	KB 30	KB 30	20	30	
2	*L* (mm)	307	120	120	22.5	22.5	120	120	22.5	22.5	120	22.5	15	120	67.5	3.1
	P (mm)	20	45	30	KB 30	KB 30	20	30	KB 30	KB 30	45	KB 30	KB 30	20	30	
3	*L* (mm)	307	120	120	15	120	22.5	22.5	22.5	120	22.5	22.5	120	120	67.5	23.4
	P (mm)	20	45	45	KB 30	30	KB 30	KB 30	KB 30	30	KB 30	KB 30	20	20	30	
4	*L* (mm)	307	120	120	22.5	120	120	22.5	22.5	120	15	22.5	22.5	120	67.5	23.4
	P (mm)	20	45	30	KB 30	45	20	KB 30	KB 30	30	KB 30	KB 30	KB 30	20	30	
5	*L* (mm)	307	120	22.5	120	22.5	120	15	22.5	120	120	22.5	22.5	120	67.5	23.4
	P (mm)	20	45	KB 30	45	KB 30	30	KB 30	KB 30	30	20	KB 30	KB 30	20	30	
6	*L* (mm)	307	120	120	22.5	120	120	22.5	22.5	22.5	120	15	22.5	120	67.5	5.9
	P (mm)	20	45	30	KB 30	45	20	KB 30	KB 30	KB 30	30	KB 30	KB 30	20	30	
7	*L* (mm)	307	120	22.5	22.5	120	120	22.5	120	22.5	15	120	22.5	120	67.5	21.3
	P (mm)	20	45	KB 30	KB 30	20	30	KB 30	30	KB 30	KB 30	45	KB 30	20	30	
8	*L* (mm)	307	120	22.5	120	22.5	22.5	22.5	15	120	120	22.5	120	120	67.5	3.0
	P (mm)	20	45	KB 30	20	KB 30	KB 30	KB 30	KB 30	30	30	KB 30	45	20	30	

Table 6. Optimal screw configurations and operating conditions for runs 9 to 12.

Point		Beginning of screw		1	2	3	4	5	6	7	8	9	10	End of screw		Q (kg/hr)	N (rpm)	T_b (ºC)
1	L (mm)	307	120	22.5	120	22.5	120	120	120	22.5	22.5	15	22.5	120	67.5	23.3	199	188
	P (mm)	20	45	KB 30	30	KB 30	30	45	20	KB 30	KB 30	KB 30	KB 30	20	30			
2	L (mm)	307	120	22.5	22.5	120	22.5	22.5	22.5	120	120	15	120	120	67.5	3.2	59	167
	P (mm)	20	45	KB 30	KB 30	30	KB 30	KB 30	KB 30	45	30	KB 30	20	20	30			
3	L (mm)	307	120	120	22.5	22.5	120	120	120	22.5	22.5	15	22.5	120	67.5	23.4	200	191
	P (mm)	20	45	45	KB 30	KB 30	20	30	30	KB 30	KB 30	KB 30	KB 30	20	30			
4	L (mm)	307	120	22.5	22.5	22.5	120	120	120	22.5	15	22.5	120	120	67.5	5.9	57	220
	P (mm)	20	45	KB 30	KB 30	KB 30	30	20	45	KB 30	KB 30	KB 30	30	20	30			
5	L (mm)	307	120	22.5	120	15	120	120	120	22.5	22.5	22.5	22.5	120	67.5	23.3	200	205
	P (mm)	20	45	KB 30	20	KB 30	30	45	30	KB 30	KB 30	KB 30	KB 30	20	30			
6	L (mm)	307	120	22.5	22.5	120	120	22.5	120	22.5	120	15	22.5	120	67.5	14.8	186	216
	P (mm)	20	45	KB 30	KB 30	30	20	KB 30	45	KB 30	30	KB 30	KB 30	20	30			
7	L (mm)	307	120	120	22.5	120	22.5	15	22.5	120	22.5	120	22.5	120	67.5	22.9	200	197
	P (mm)	20	45	45	KB 30	30	KB 30	KB 30	KB 30	20	KB 30	30	KB 30	20	30			
8	L (mm)	307	120	120	22.5	120	120	120	15	22.5	22.5	22.5	22.5	120	67.5	3.1	200	198
	P (mm)	20	45	45	KB 30	30	20	30	KB 30	KB 30	KB 30	KB 30	KB 30	20	30			

Table 7 shows the optimized values of the different objectives for the three groups of runs, i.e., when more degrees of freedom for the optimization are progressively allowed. For example, a considerable gain is obtained for output and average strain when geometrical and operating parameters are used at once for the optimization. In group 1, output was defined as 10 kg/hr, which is far from the maximum attainable value (circa 23 kg/hr). When Q also became an optimization variable (groups 2 and 3), output improved significantly. Also, T_{exit}, *SME* and viscous dissipation minimization from group 2 improved 12.6, 64.1 and 3.7%, respectively, to group 3.

Table 7. Best results of the objectives for groups 1 to 3.

Objectives	**Group 1**		**Group 2**			**Group 3**		
	value	**run**	**value**	**run**	**variation (%)**	**value**	**run**	**variation (%)**
***CR* (%) -** *Maximization*	99.9	1	99.9	5-8	0.0	99.9	9-12	0.0
***Q* (kg/hr) -** *Maximization*	10	1-4	23.3	5	133.0	23.3	9	133.0
T_{exit} (ºC) - *Minimization*	196.3	1	192.6	5	1.8	171.5	9	12.6
***SME* (MJ/kg) -** *Minimization*	1.447	2	1.221	6	15.6	0.52	10	64.1
T_{max}/T_b - *Minimization*	1.09	3	1.13	7	-3.7	1.05	11	3.7
***AvgStrain* -** *Maximization*	4517	4	10067	8	122.9	9921	12	119.6

Finally, Figure 8 shows the influence of the $[M_0]/[I_0]$ ratio on the optimization results. In order to generate the data, runs 9 and 10 of Table 10 were repeated, but using different values of the $[M_0]/[I_0]$ ratio (400 and 800, respectively). The Figure shows the optimal Pareto frontiers in the objectives domain, taking into account that output is used both as decision variable and as an objective to be maximized. As seen above, an increase in $[M_0]/[I_0]$ induces a slower reaction. Consequently, to reach the desired conversion ratio, the barrel temperature has to be raised, mainly when operating at high outputs, as the total residence time is shorter. The screw speed should also be increased in order to promote viscous heating; however, this yields a higher exit temperature and a higher SME. The screw speed/output correlation is

independent of the $[M_0]/[I_0]$ ratio. The minimization of the SME (run 10) is obtained at the cost of increasing the barrel temperature (to reduce the viscosity), almost independently of the value of the $[M_0]/[I_0]$ ratio.

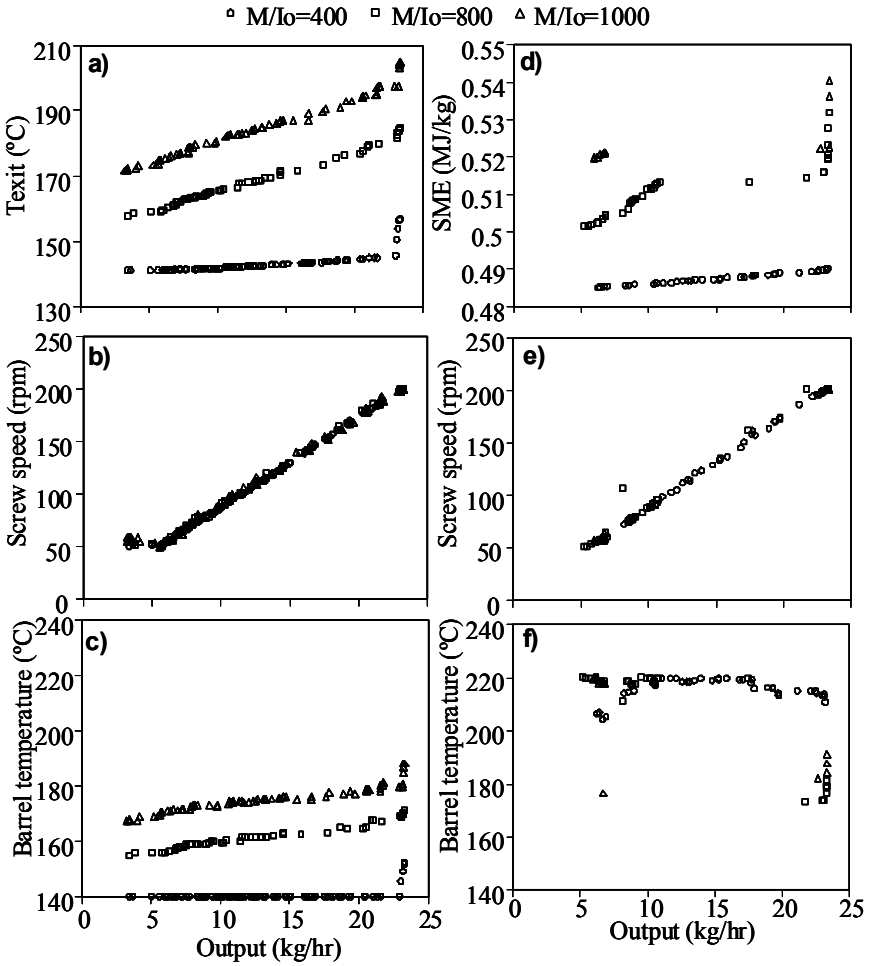

Figure 8. Influence of the $[M_0]/[I_0]$ ratio on the optimization results. Run 9: a) to c); Run 10: d) to f).

Table 8. Individual screw elements used for the optimization of starch cationization (LH indicates a left-handed screw element, KB denotes a block of kneading discs).

Element	Beginning of screw		**1**	**2**	**3**	**4**	**5**	**6**	**7**	**8**	**9**	**10**	**11**	**12**	**13**	**14**	**15**	**16**	End of screw
L (mm)	250	50	50	50	50	25	25	50	50	50	25	25	25	25	50	25	25	25	25
P (mm)	33.3	25	16.6	KB -45º	33.3	25	LH 16.6	16.6	KB -45º	33.3	25	LH 16.6	25	16.6	KB -45º	25	16.6	LH 12.5	16.6

3.3 Starch Cationization

Starch Cationization will take place in a Clextral BC21 (Clextral, France) laboratory scale co-rotating twin screw extruder (screw length of 900 mm). Table 8 presents the individual elements that are available to assemble the screws. As for the Leistritz extruder, those elements close to the hopper and to the screw tip were retained in their original location. The reagent is injected at the end of the second element, i.e., at an axial distance of 300 mm.

Seven optimization runs were carried out as illustrated in Table 9, which identifies the decision variables (i.e., the parameters to be optimized) and the optimization objectives. The aim and range of variation of the latter are shown in Table 10. A restriction to the maximum achievable temperature was always applied (T_{Max} < 165ºC), while for run 7 the solutions were only taken as valid when SME was lower than 0.72 MJ/kg. In every case, the screw speed N, the barrel temperature T_b, the reagent injection point and its amount were kept constant and equal to N = 400 rpm, T_b = 130 ºC, 300 mm and 0.107 Q_{starch}, respectively, where Q_{starch} is the starch feed rate. As explained above, the concentration of reagent can be expressed as a theoretical degree of substitution (DS_{th}). It was also explained that since a starch glycosil unit has three hydroxyl groups, the maximum degree of substitution DS is 3. Although the cationic starches used in the paper industry usually have DS values in the range 0.02-0.05, the value of 0.1 for DS_{th} was selected because it is more difficult to reach and, henceforth, the optimization exercise is more interesting.

Table 9. Optimization runs for starch cationization.

Run	Decision Variables		Objectives
	Q **(kg/hr)**	**Screw Configuration**	
1	2.5	16 elements	*RE, SME*
2	5		
3	10		
4	20		
5	40		
6	[2.5-40]	16 elements	*RE, SME*
7	[2.5-40]	16 elements	*RE, Q*

Runs 1 to 5 involve the optimization of the screw geometry for different values of output, taking into consideration the reaction efficiency (RE) and the specific mechanical energy (SME), which are to be maximized and minimized, respectively (Table 10). In contrast, runs 6 and 7 tackle at the same time the screw configuration and output optimization, now in order to maximize RE and minimize SME (run 6), or maximize output Q (run 7).

Table 10. Optimization objectives, aim of optimization and range of variation.

Objectives	**Aim**	**Range of variation**
Output (Q), kg/hr	Maximize	[2.5-40]
Specific Mechanical Energy (*SME*), MJ/kg	Minimize	[0-1.5]
Reaction Efficiency (*RE*), %	Maximize	[0-100]

Figure 9 shows the initial population and the non-dominated solutions of the 30th population for runs 1 to 5. As before, the algorithm is able to evolve towards better solutions along the successive generations. As expected, an increase in output implies necessarily a decrease in the reaction level (i.e., *RE* decreases), regardless of the screw configuration (which was also optimized). The corresponding screw configurations (for maximizing *RE*) in these 5 runs are described in Table 11. In all cases, the optimization algorithm places the left handed (LH) element as upstream as possible (positions 1 or 2), in order to melt rapidly the starch. The remaining restrictive elements are located mostly at positions 13 to 16. In contrast, the minimization of SME is achieved mainly as a result of the higher melt temperature (thus lower viscosity) resulting from higher outputs.

The various optimal Pareto frontiers obtained for different outputs seem to define an asymptotic limiting curve in Figure 9. This should be confirmed by run 6, which comprises the optimization of output together with that of screw configuration. Figure 10 presents the Pareto frontiers in the objectives domain for runs 6 and 7. In fact, the shape of the Pareto frontier for run 6 is identical of that of runs 1 to 5.

Table 12 presents the screw configurations for the solutions 1 to 4 in Figure 10. Again, the optimal screws have a restrictive element (left handed) at the beginning of the screw (position 2), in order to melt the starch as soon as possible. Screws 1 and 2, where the aim is to minimize *SME*, are apparently similar in geometrical terms, but can attain quite different output levels (3 and 39 kg/hr, respectively). These results are in accordance with those for runs 1 to

5, since the lowest SME is obtained at high outputs, when the temperatures are also high and, consequently, the viscosity is lower.

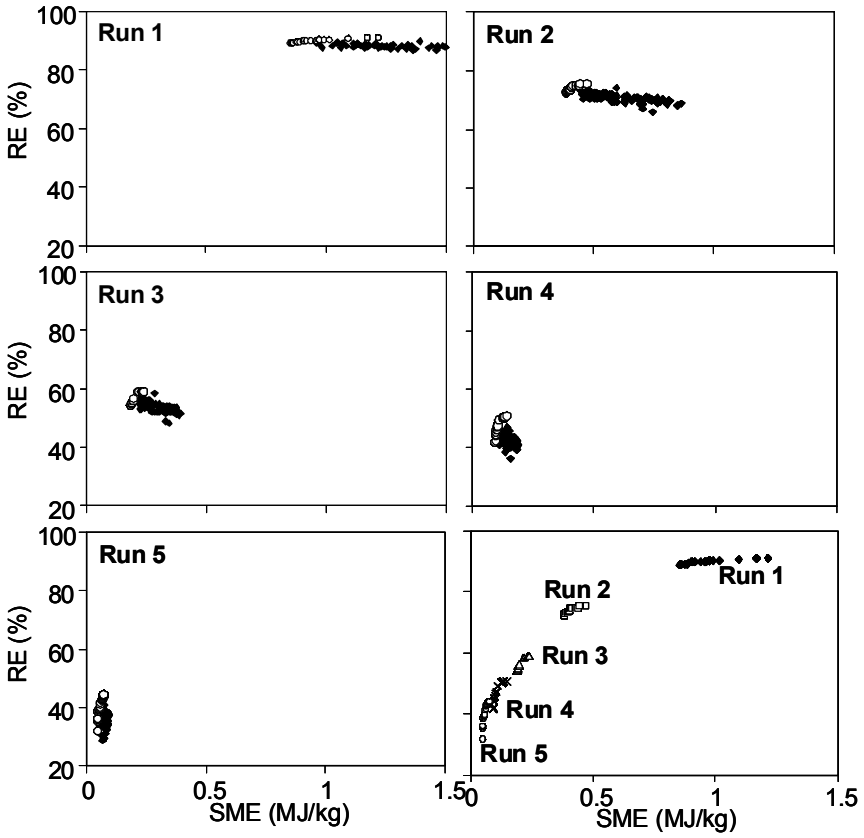

Figure 9. Optimizing starch cationization. Initial population and non-dominated solutions at the 30th generation, runs 1 to 5.

Run 7 involves a distinct optimization exercise. In the case of the screw configurations that maximize the feed rate (point 4 in Figure 10 and Table 12), it is advisable to locate the restrictive elements as downstream as possible. Such a screw geometry should maximize the melt temperature increase due to viscous heating, which might balance the reduction in residence time that results from increasing outputs. Conversely, the screw profiles maximizing RE yield low outputs (around 3 kg/h) and have a very different construction:

Table 11. Optimal screw configurations maximizing *RE* of starch cationization, runs 1 to 5.

		Beginning of screw		**1**	**2**	**3**	**4**	**5**	**6**	**7**	**8**	**9**	**10**	**11**	**12**	**13**	**14**	**15**	**16**	End of screw
Run 1	L (mm)	250	50	25	25	50	25	50	25	25	50	50	50	25	25	25	50	50	25	25
	P (mm)	33.3	25	25	LH 12.5	33.3	16.6	16.6	16.6	25	16.6	33.3	KB -45º	25	25	LH 12.5	KB -45º	KB -45º	LH 16.6	16.6
Run 2	L (mm)	250	50	25	25	25	25	50	50	25	25	50	50	25	50	25	50	50	25	25
	P (mm)	33.3	25	16.6	LH 12.5	25	25	16.6	33.3	25	LH 16.6	33.3	16.6	16.6	KB -45º	25	KB -45º	KB -45º	LH 12.5	16.6
Run 3	L (mm)	250	50	25	50	25	25	25	25	50	50	25	50	25	25	25	50	50	50	25
	P (mm)	33.3	25	LH 12.5	16.6	16.6	25	25	25	33.3	16.6	16.6	33.3	LH 16.6	25	LH 12.5	KB -45º	KB -45º	KB -45º	16.6
Run 4	L (mm)	250	50	25	25	50	50	25	25	50	25	25	50	25	50	50	25	25	50	25
	P (mm)	33.3	25	25	LH 16.6	33.3	16.6	25	16.6	16.6	25	25	KB -45º	16.6	33.3	KB -45º	LH 12.5	LH 12.5	KB -45º	16.6
Run 5	L (mm)	250	50	25	50	25	50	25	50	50	25	25	50	50	25	25	25	50	25	25
	P (mm)	33.3	25	LH 16.6	33.3	25	33.3	16.6	16.6	KB -45º	25	25	KB -45º	16.6	16.6	25	LH 12.5	KB -45º	LH 12.5	16.6

Table 12. Optimal screw configurations for starch cationization, runs 6 and 7.

Point		Beginning of screw		1	2	3	4	5	6	7	8	9	10	11	12	13	14	15	16	End of screw
1	L (mm)	250	50	25	25	25	25	50	25	50	50	25	50	25	25	50	50	25	50	25
	P (mm)	33.3	25	16.6	LH 12.5	16.6	25	33.3	25	16.6	33.3	25	KB -45º	25	LH 16.6	KB -45º	16. 6	LH 12.5	KB -45º	16.6
2	L (mm)	250	50	25	25	25	50	50	25	25	25	50	25	25	50	25	50	50	50	25
	P (mm)	33.3	25	16.6	LH 12.5	25	33.3	33.3	16.6	25	25	16. 6	LH 16.6	25	KB -45º	LH 12.5	KB -45º	16. 6	KB -45º	16.6
3	L (mm)	250	50	25	25	25	25	50	50	25	25	25	50	50	25	50	50	50	25	25
	P (mm)	33.3	25	25	LH 12.5	25	LH 16.6	33.3	33.3	25	16.6	25	KB -45º	16.6	16.6	16.6	KB -45º	KB -45º	LH 12.5	16.6
4	L (mm)	250	50	25	25	25	50	50	25	50	50	25	25	25	50	25	50	50	25	25
	P (mm)	33.3	25	25	LH 12.5	25	33.3	33.3	16.6	16.6	16.6	25	16.6	25	KB -45º	LH 16.6	KB -45º	KB -45º	LH 12.5	16.6

the restrictive elements are generally separated by conveying elements and are located near to the melting section.

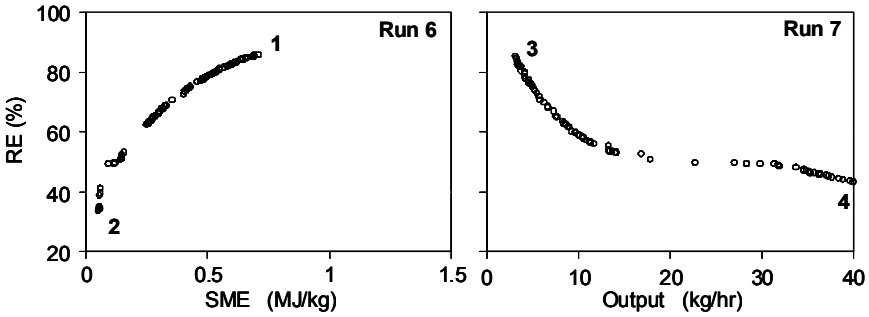

Figure 10. Optimal Pareto frontiers for starch cationization, runs 6 and 7.

4 Conclusion

The optimization studies presented in this chapter demonstrated the potential of multi-objective evolutionary algorithms for optimizing the screw configuration and the processing conditions for specific applications in reactive extrusion, an important technology used to generate advanced polymer systems. The use of a Reduced Pareto Set Genetic Algorithm enabled the identification of feasible solutions, with satisfactory physical sense, even when conflicting objectives were selected.

References

[1] Xanthos M. *Reactive Extrusion: Principles and Practice*; Hanser: Munich (1992).

[2] Baker, W., Scott, C., Hu, G.H. *Reactive Polymer Blending*; Hanser: Munich (2001).

[3] Cassagnau, P., Bounor-Legaré, V., Fenouillot, F. *Intern Polym Proc*. 2007, *22*, 218-258.

[4] Vergnes, B., Berzin, F. *Plast., Rubber, Comp.: Macromol. Eng*. 2004, *33*, 409-415.

[5] Valette, R., Coupez, T., Vergnes, B. (2008) Proceedings 24th Annual Meeting of the Polymer Processing Society, CD Rom.

[6] Berzin, F. Hu G.H. In *Techniques de l'Ingénieur*, AM 3654, Paris, 2004, 1-16.

[7] Jongbloed, H.A., Kiewiet, J.A., Van Dijk, J.H., Janssen, L.P.B.M. *Polym. Eng. Sci*. 1995, *35*, 1569-1579.

[8] Vergnes, B., Della Valle, G., Delamare, L. *Polym. Eng. Sci*. 1998, *38*, 1781-1792.

[9] Vergnes, B., Souveton, G., Delacour, M.L., Ainser, A. *Int. Polym. Proc*. 2001, *16*, 351-362.

[10] Carneiro, O.S., Covas, J.A., Vergnes, B., J. *Appl. Polym. Sci*. 2000, *78*, 1419-1430.

[11] F. Berzin, F., Vergnes, B., Lafleur, P.G., Grmela, M. *Polym. Eng. Sci*. 2002, *42*, 473-481.

[12] Lozano, T., Lafleur, P.G., Grmela, M., Vergnes, B. *Intern. Polym. Proc*. 2003, *18*, 12-19.

[13] Delamare, L., Vergnes, B., *Polym. Eng. Sci*. 1996, *36*, 1685-1693.

[14] C. Teixeira, R. Faria, J.A. Covas, A. Gaspar-Cunha, Modelling Flow and Heat Transfer in Co-Rotating Twin-Screw Extruders, 10th Esaform Conference on Material Forming, E. Cueto and F. Chinesta Editors, Zaragoza, Spain, April, 907, 957 2007.

[15] Poulesquen, A., Vergnes, B., Cassagnau, Ph., Gimenez, J., Michel, A. *Intern. Polym. Proc*. 2001, *16*, 31-38.

[16] Berzin, F., Vergnes, B., Dufossé, P., Delamare, L., *Polym. Eng. Sci*. 2000, *40*, 344-356.

[17] Berzin, F., Vergnes, B., Canevarolo, S.V., Machado, A.V., Covas, J.A. *J. Appl. Polym. Sci*. 2006, *99*, 2082-2090.

[18] Berzin, F., Vergnes, B., *Intern. Polym. Proc*. 1998, *13*, 13-22.

[19] Berzin, F., Tara, A., Tighzert, L., Vergnes, B. *Polym. Eng. Sci*. 2007, *47*, 112-119.

[20] Berzin, F., Tara, A., Vergnes, B.*, Polym. Eng. Sci*. 2007, *47*, 814-823.

[21] Chalamet, YI., Taha, M. Berzin, F., Vergnes, B. *Polym. Eng. Sci*. 2002,

42, 2317-2327.

[22] Dubois, Ph., Ropson, N., Jérôme, R., Teyssié, Ph., *Macromol*. 1996, *29*, 1965-1975.

[23] Gimenez, J., Boudris, M., Cassagnau, Ph., Michel, A., *Polym. React. Eng*. 2000, *8*, 135-157.

[24] Gimenez, J., Boudris, M., Cassagnau, Ph., Michel, A., *Intern. Polym. Proc*. 2000, *15*, 20-27.

[25] Gimenez, J., Cassagnau, Ph., Fulchiron, R., Michel, A., Macromol. Chem. Phys. 2000, 201, 479-490.

[26] Gimenez, J., Cassagnau, Ph., Michel, A. *J. Rheol*. 2000, *44*, 527-548.

[27] Solarek, D.B. In *Modified Starches: Properties and Uses*, Würzburg, O.B;. Ed.; CRC Press: Boca Raton, FL, 1986, Chap. 8.

[28] Rutenberg, M.W., Solareck, D.B. In *Starch Derivatives: Production and Uses*, Whistler, R.L., BeMiller, J.N., Paschall, E.F., Eds.; Starch: Chemistry and Technology, 2nd ed., Academic Press: Orlando, FL, 1984; Chap. 10.

[29] Tara, A., Berzin, F., Tighzert, L., Vergnes, B., *J. Appl. Polym. Sci*. 2004, 93, 201-208.

[30] Ayoub, A., Berzin, F., Tighzert, L., Bliard, C. *Starch* 2004, *56*,513-519.

[31] Berzin, F., Tara, A., Tighzert, L. *Appl. Rheo*. 2007, 17, 1-7.